Projected changes to South Atlantic boundary currents and confluence region in the CMIP5 models: the role of wind and deep ocean changes

2016 Environ. Res. Lett. 11 094013

(http://iopscience.iop.org/1748-9326/11/9/094013)

Environmental Research Letters

LETTER

Projected changes to South Atlantic boundary currents and confluence region in the CMIP5 models: the role of wind and deep ocean changes

G M Pontes[1], A Sen Gupta[2] and A S Taschetto[2]

[1] School of Oceanography, State University of Rio de Janeiro (UERJ), Rio de Janeiro, Brazil
[2] Climate Change Research Centre and Australian Research Council (ARC) Centre of Excellence for Climate System Science, The University of New South Wales, Australia

E-mail: gabriel.pontes@uerj.br

Keywords: South Atlantic ocean, climate change, Climate Model Intercomparisson Project-CMIP, Sverdrup's dynamics, Brazil current, Brazil–Malvinas confluence, water masses

Supplementary material for this article is available online

OPEN ACCESS

RECEIVED
27 April 2016

REVISED
10 August 2016

ACCEPTED FOR PUBLICATION
19 August 2016

PUBLISHED
14 September 2016

Abstract

The South Atlantic (SA) circulation plays an important role in the oceanic teleconnections from the Indian, Pacific and Southern oceans to the North Atlantic, with inter-hemispheric exchanges of heat and salt. Here, we show that the large-scale features of the SA circulation are projected to change significantly under 'business as usual' greenhouse gas increases. Based on 19 models from the Coupled Model Intercomparison Project phase 5 there is a projected weakening in the upper ocean interior transport (<1000 m) between 15° and ~32°S, largely related to a weakening of the wind stress curl over this region. The reduction in ocean interior circulation is largely compensated by a decrease in the net deep southward ocean transport (>1000 m), mainly related to a decrease in the North Atlantic deep water transport. Between 30° and 40°S, there is a consistent projected intensification in the Brazil current strength of about 40% (30%–58% interquartile range) primarily compensated by an intensification of the upper interior circulation across the Indo-Atlantic basin. The Brazil–Malvinas confluence is projected to shift southwards, driven by a weakening of the Malvinas current. Such a change could have important implications for the distribution of marine species in the southwestern SA in the future.

1. Introduction

The southwestern South Atlantic (SA) is one of the world's most energetic oceanic regions. This is a result of the meeting of two intense opposing flows: the poleward Brazil current (BC) and the equatorward Malvinas current (MC), to form the most important oceanographic front in the SA: the Brazil–Malvinas confluence (BMC; figure S1).

The BMC strongly influences the local climate and biological environment. The large sea surface temperature (SST) gradient affects local surface winds and heat advection to adjacent coastal areas (De Camargo *et al* 2013). Frontal zones are characterized by high primary production that enhances the local food chain (Alemany *et al* 2014).

This study will examine projected changes and driving factors for the SA circulation. The large-scale ocean circulation can, to some extent, be broken down into a surface wind-driven circulation and a deep density-driven overturning circulation. The surface circulation can reach 1000–2000 m depending on the region. Of particular importance are the western boundary currents (WBCs) that transport large amounts of salt, heat, and other tracers poleward. The basin interior surface flow usually opposes the WBC, partially compensating its poleward mass flux. These flows are also affected by air-sea fluxes, inter-basin transport and vertical transport from below associated with the meridional overturning circulation.

In the SA, the BC extends between about 20 and 40°S (figure S1) with considerable transport variation

along its length. Generally, its transport north of 25°S is less than 10 Sv (Peterson and Stramma 1991) increasing substantially south of 30°S. Depth integrated transport to 1400–1500 m around 38°S might reach 19 Sv based on geostrophic estimates (Gordon and Greengrove 1986). Table S1 summarizes previous transport estimates.

The BMC is situated at around 38°S and shows seasonal variability with meridional shifts of about 5° (Wainer *et al* 2000, Goni *et al* 2011). A number of mechanisms have been proposed to explain the seasonal BMC movements, including variations in BC transport (Olson *et al* 1988), MC transport (Matano 1993), Antarctic Circumpolar current (ACC) transport (Gan *et al* 1998), and seasonal wind stress changes (Fetter and Matano 2008). There is also evidence of longer-term change in the confluence location with both observational data (Goni *et al* 2011) and numerical simulations (Combes and Matano 2014) indicating a southward shift at a rate of between 0.39° and 0.81° per decade over the last two decades. The primary drivers of this change remain a topic of research.

Many studies have used coupled atmosphere-ocean general circulation models (AOGCM) to investigate changes in oceanic and atmospheric circulation in Global Warming scenarios. One robust change evident in both observations (Hill *et al* 2008, Wu *et al* 2012) and climate simulations (Wainer *et al* 2004, Sen Gupta *et al* 2009, 2016) is an intensification and poleward shift of portions of the subtropical gyres associated with an intensification of the WBCs or their extensions. This has been related to long-term changes in the wind stress curl (WSC), associated with changes in ozone and CO_2 forcing (e.g. Saenko *et al* 2005, Polvani *et al* 2011). Robust changes in the large-scale atmosphere circulation are also projected by climate models including a widening and slowing down of the Hadley cell and poleward shift of the Southern Hemisphere westerlies (Lu *et al* 2007, Harvey *et al* 2014).

The aim of this study is to examine the projected changes to SA ocean circulation by analyzing output from the Coupled Model Intercomparison Project phase 5 (CMIP5) models (Taylor *et al* 2012). In particular, we examine changes in the SA basin circulation in relation to projected changes in surface winds and the large-scale overturning circulation and their consequences for the WBCs and BMC.

2. Climate models and methods

CMIP5 models include state-of-the-art AOGCM and Earth System Models that were used to inform the Intergovernmental Panel on Climate Change Fifth Assessment Report. Typically, ocean horizontal resolution is approximately 1.0° × 1.0° although there is considerable inter-model differences (table S2). As a result, these models do not explicitly resolve mesoscale processes, although the effects of these processes are included through parameterisation. The vertical ocean resolution varies between 31 and 70 layers.

We used output from 19 CMIP5 models (table S2), which have the available variables and scenarios for the current study. To examine projected changes we have made comparisons between the *historical* simulations that covers 1850–2005 and a *high emissions* scenario (*RCP8.5*) that extends the historical simulation to 2100. Historical simulations are forced by observationally derived data of the major climate forcings (greenhouse gases, anthropogenic and volcanic aerosols, ozone and solar irradiance). In the *RCP8.5* scenario greenhouse gas forcing increases throughout the 21st century reaching an additional radiative forcing of about 8.5 W m^{-2}, equivalent to ~1370 CO_2-equivalent at the end of the century (Taylor *et al* 2012). A single ensemble member is used from each model (i.e. the first member with all available variables; usually *r1i1p1*). Variables from both ocean and atmospheric components were used: mass transport (*umo* and *vmo)* and wind stress (*tauu* and *tauv)*. When mass transport variables were not available, we calculated mass transport from velocity fields (*uo* and *vo*). Despite long spin-up integrations some model drift may remain in the subsurface fields, however this is likely small compared to forced trends, particularly when considering ensemble averages (Sen Gupta *et al* 2016) and so has been neglected.

To estimate the state of the ocean during the 20th century the data was averaged over the period 1900–2000 from the *historical* simulations. In order to examine the projected changes, the averaged 2050–2100 period from the *RCP8.5* simulations was compared with the 20th century state.

The calculation of the WBC transports is problematic as there are differences in their representation across models due to different bathymetries, coastlines, and resolutions. As a result we have manually selected the eastern boundary of the WBC for each model as the longitude where meridional poleward flow and any associated weak offshore counter flow vanishes in the long term mean velocities (see example in figure S2; following Sen Gupta *et al* 2016). The counter current is included as we are interested in identifying the western limit of the interior flow (that extends across the remainder of the basin) that can be related to Sverdrup transport. In most of the models the BC does not extend deeper than 1000 m, as a result we use this depth to define upper ocean transports. This is consistent with observations reported by Gordon and Greengrove (1986) who showed that most of the transport occurs in the upper 800 m.

The statistical significance of projected changes has been determined by applying the Robust Rank Test (Fligner and Policello 1981) to examine if two distributions have equal medians and are indicated in table S5. Unless otherwise stated, all values presented

are multi-model medians (MMM) and associated interquartile range (IQR).

3. Results

3.1. Basin interior and WSC

The upper-ocean interior circulation in the SA is estimated as the meridional volume transport shallower than 1000 m integrated from the eastern edge of WBC to the African coast (or east to the next land boundary south of Africa). The zonally integrated 20th century MMM equatorward interior transport decreases almost linearly towards the north from 27.5 Sv (23.7 to 29.1 Sv) at 30°S to zero at about 16°S (figure 1(a); individual model tranports, inter-quartile ranges and MMM are collated in table S5 for all results). North of this, the interior flow is weakly southwards.

Between 17 and ~30°S, all but one model project a decrease in the basin interior transport strength. The MMM decrease is statistically significant at the 95% level between 13°S and 32°S (figure 1(b)). The change in the interior transport is largest at 23°S (21°–25°S). In this region, there is a mean projected weakening in transport of ~3 Sv (2.4–3.4 Sv) corresponding to a 22% decrease (16%–24%). In this same region (between 21° and 25°S), there is no significant change in the BC transport (figures 1(b) and 2(a); see section 3.3). Thus, the MMM weakening in the ocean interior transport is not compensated by an associated weakening of the WBC.

To help understand the cause of the circulation change we examine the zonally averaged WSC integrated over the SA basin (or east to the next land boundary south of Africa; figures 1(c) and (d)). The WSC can be related via Sverdrup theory to the basin interior transport (positive/negative WSC implies a net northward/southwards interior transport). As the CMIP5 models have coarse resolution, we have linearly interpolated the zonally averaged WSC to 0.1° resolution and estimated the latitude of the maximum WSC by calculating the WSC weighted mean latitude based on latitudes where WSC was greater than 50% of its maximum. The WSC maximum is located around 38.4°S in the models (36.4°–39.4°S; figure 1(c)). Comparison with observations (ERA-Interim reanalysis from 1979 to 2013) shows that the latitude of the MMM WSC maximum is biased polewards by ~2.9° (figure 1(c)). This is despite the fact that further south there is a distinct equatorwards bias in the maximum zonal winds, consistent with previous studies (i.e. Barnes and Polvani 2013, Bracegirdle *et al* 2013).

All of the models project a southward shift in both maximum WSC and WSC zero line. The poleward shift in the position of the maximum WSC is 1.4° (1.2°–2.4°; figure 1(c)). The MMM WSC zero line is located at about 51.2°S (50.2°–52.2°S) and is projected to move southward by about 1.6° (1.1°–2.1°; consistent with Cai *et al* 2005, Saenko *et al* 2005, Wu *et al* 2012). The latter identified a 2° southward shift in the circumpolarly averaged WSC, associated with a doubling of CO_2 in a single climate model.

Figure 1(b) reveals a strong correspondance between interior and Sverdrup transport changes (north of the southern tip of Africa), associated with a WSC weakening over this region (figure 1(d)). A strong inter-model correlation ($r = 0.8$, $p < 0.05$) between Sverdrup transport at 25°S and the associated model interior transport changes indicates that inter-model differences in the projected changes are well explained by differences in the projected surface wind changes (table 1).

3.2. Deep circulation

The 20th century deep meridional transport (integrated net transport below 1000 m) is almost constant along the SA (figure 1(a)) with a mean transport of −15.9 Sv (−18.2 to −12.9 Sv). Given that there is a net projected change in the upper ocean circulation (i.e. the BC and interior changes do not compensate each other north of the southern tip of Africa) and the Atlantic Basin is closed to the north, there must be a compensating change in the deep ocean circulation. Indeed, all models project a weakening of the deep transport in the 21st century. The net MMM SA deep circulation decreases significantly by approximately 3.4 Sv (~2–5 Sv; figure 1(b)) corresponding to a 19% weakening (14%–28%).

We examine whether this weakening can be related to changes in the southward flowing North Atlantic deep water (NADW) and northward flowing Antarctic bottom water (AABW) entering the Atlantic basin at 33°S. To quantify this we have defined NADW as the southward transport below 1000 m between the South American coast and 40°W (figure 2(b)). The AABW transport is defined as any northward flux on the western side of the basin (west of 20°W) and below 3000 m (figure 2(b)). Based on these definitions, the NADW transport is −20.8 Sv (−22.8 to −19.3 Sv; figure S3) for the *historical* period. This value is similar to the estimated by Garzoli *et al* (2015) of −19.5 Sv (5.4) based on observations at 35°S. All but one model (NorESM1-M) suggest that NADW transport will decrease by 2.4 Sv (1.7–3.5 Sv; table S5) corresponding to a 13% reduction (8%–14%).

The AABW transport for the 20th century is 5.5 Sv (3.8–8.5 Sv; figure S3). While there is a MMM projected decrease of 0.6 Sv (−1.4 to 0.1 Sv), the change is not statistically significant with 13 out of 19 models projecting a weakening.

As such, the NADW plays the dominant role in the net deep southward transport decrease and in balancing most of the mismatch between surface interior and BC transport changes. It is interesting that most models also show a net northward projected change at about 10°W and 25°W (figure 2(c); albeit considerably

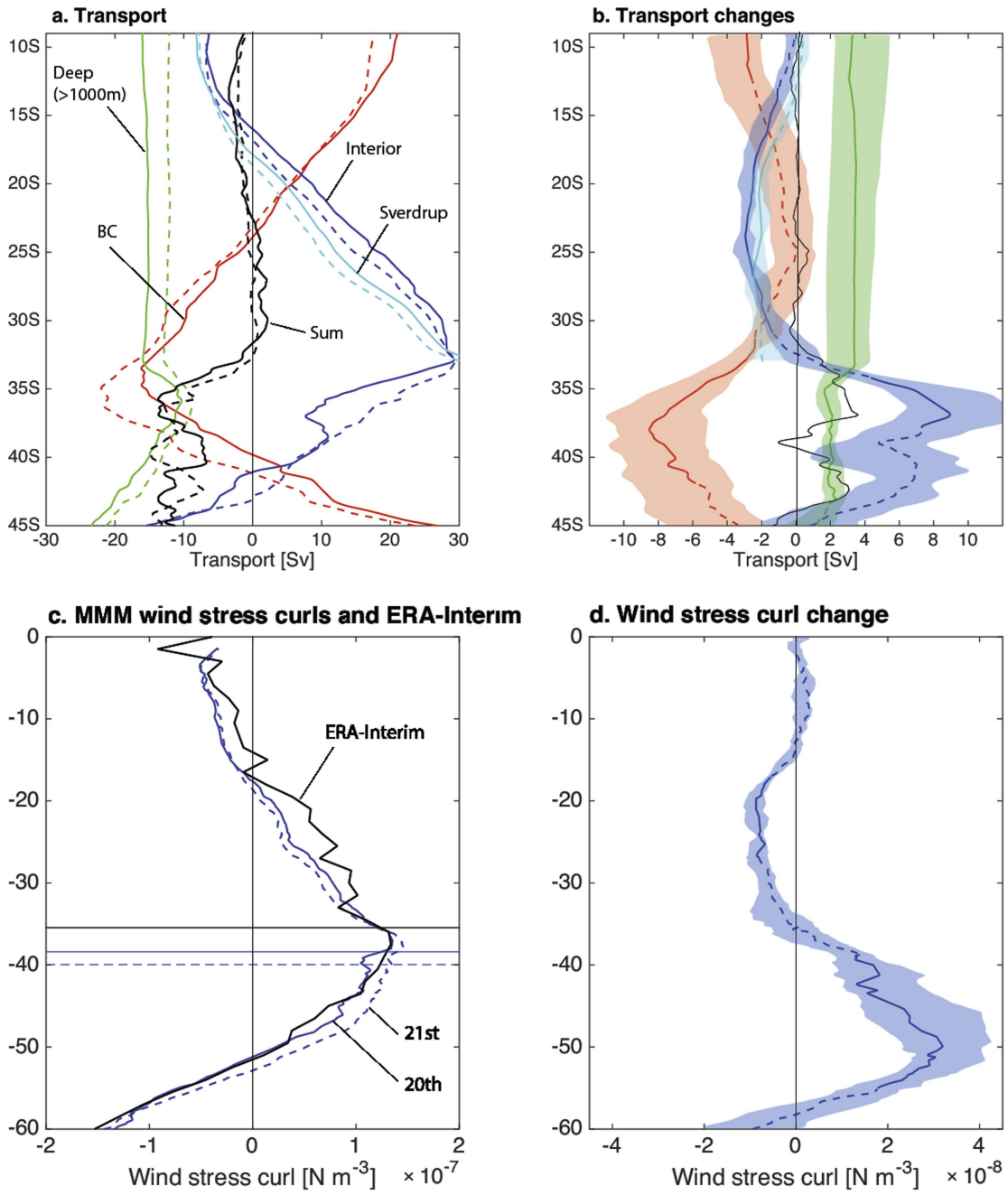

Figure 1. (a) Multi-model median transport of BC, basin interior (below the southern tip of Africa it is integrated to the next landmass—Australia, New Zealand or South America), wind stress-derived Sverdrup transport, and deep circulation (>1000 m) and the sum of BC, interior and deep transports. Averaged from 1900 to 2000 (solid lines) and from 2050 to 2100 (dashed lines). (b) Multi-model median transport change (RCP8.5 minus historical), solid line indicates where the change is significant at the 95% level. (c) Multi-model median zonally averaged wind stress curl, averaged from 1900 to 2000 (20th), and from 2050 to 2100 (21st), and ERA-Interim averaged from 1979 to 2013. Horizontal lines indicate the associated maximum wind stress curl position calculated from the weighted averaged method. (d) Zonally averaged (in between landmasses when south of the tip of Africa) wind stress curl change, solid line indicates where the change is significant at the 95% level. Banding indicates interquartile range based on 19 models (table S2).

weaker than the WBC change). This may relate to a weakening in parts of the NADW that have separated away the South American coastline (figure 2(b)) as a result of interaction with Vitoria-Trindade Ridge at 20°S (Garzoli *et al* 2015).

3.3. Western boundary currents

All models simulate the BC between approximately 20° and 40°S. The MMM maximum transport (based on each model's maximum transport which occurs at different latitudes) is –20.1 Sv (−23.0 to –13.2 Sv). Here, we have applied the same interpolation as for WSC (see section 3.1) for the integrated transport along the western boundary. The maximum transport latitude is 33.3°S (31.8–34.9°S, figure S4). Observational estimates around this region lie within the model range (19.2 Sv, Stramma 1989; 16 Sv, Lentini *et al* 2006, 23 Sv, Garzoli 1993, see figure S4 and table S1).

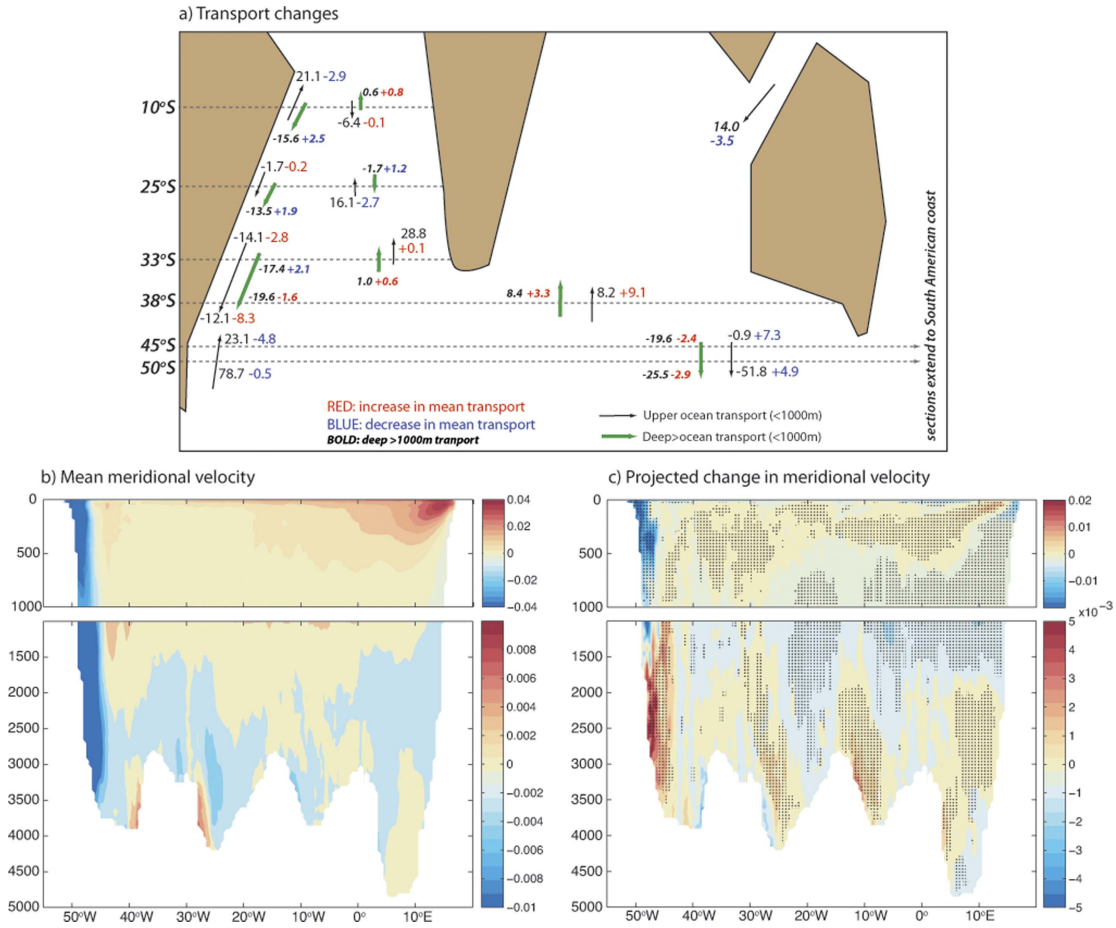

Figure 2. (a) Multimodel median transport and projected changes at selected latitudes. Black arrows represent upper ocean (<=1000 m) transport, green arrows represent deep ocean (>1000 m) transport. Black numbers indicate 20th century median transports (Sv). Interior transports are calculated across all basins for 45°S and 50°S, across Indo-Atlantic for 38°S and across the Atlantic for <=33°S. The length of the arrows is merely schematic. (b) Multi-model mean meridional velocity at 33°S (m s^{-1}) and (c) associated projected change. Stippling on panel (c) indicates regions where there is 70% agreement on sign of change.

Table 1. Correlation coefficients between Western boundary current (NBC, BC or MC) transport and compensating transports (columns 3–6) and between upper ocean interior transport and associated Sverdrup transport (column 7). Bold coefficients means a significant correlation at the 95% level ($p < 0.05$). H: historical simulation. Δ: RCP8.5 projected change.

		WBC correlation				
		Interior	NADW	>1000 m	ITF	Interior-Sverdrup correlation
10°S NBC	H	**0.7**	**0.86**	0	—	**0.7**
	Δ	0.1	**0.95**	**0.5**	—	**0.74**
25°S BC	H	**0.57**	**0.65**	0.05	—	**0.82**
	Δ	**0.61**	**0.57**	**0.4**	—	**0.81**
33°S BC	H	**0.78**	0.19	**0.58**	—	**0.52**
	Δ	**0.81**	0.34	0.1	—	**0.66**
38°S BC	H	**0.96**	**−0.69**	**0.81**	0.25	0.34
	Δ	**0.95**	0.12	0	−0.3	0.18
45°S MC	H	**0.95**	—	**0.44**	—	0.15
	Δ	**0.95**	—	0.1	—	0.1
50°S MC	H	**0.96**	—	**0.49**	—	0.08
	Δ	**0.67**	—	0.1	—	0.05

There is a projected increase in the strength of the BC along its length (figures 1(a) and (b)). Between 20° and 30°S, the BC intensification is weak and not statistically significant, even with 14 of 19 models projecting an increased transport. South of 30°S all models agree on the intensification although the magnitude varies considerably. Averaged between 30° and 40°S the increase ranges between 4.8 and 8.1 Sv (IQR) with a MMM increase of ~6 Sv. This corresponds to a substantial 40% (30%–58%) increase in mean transport.

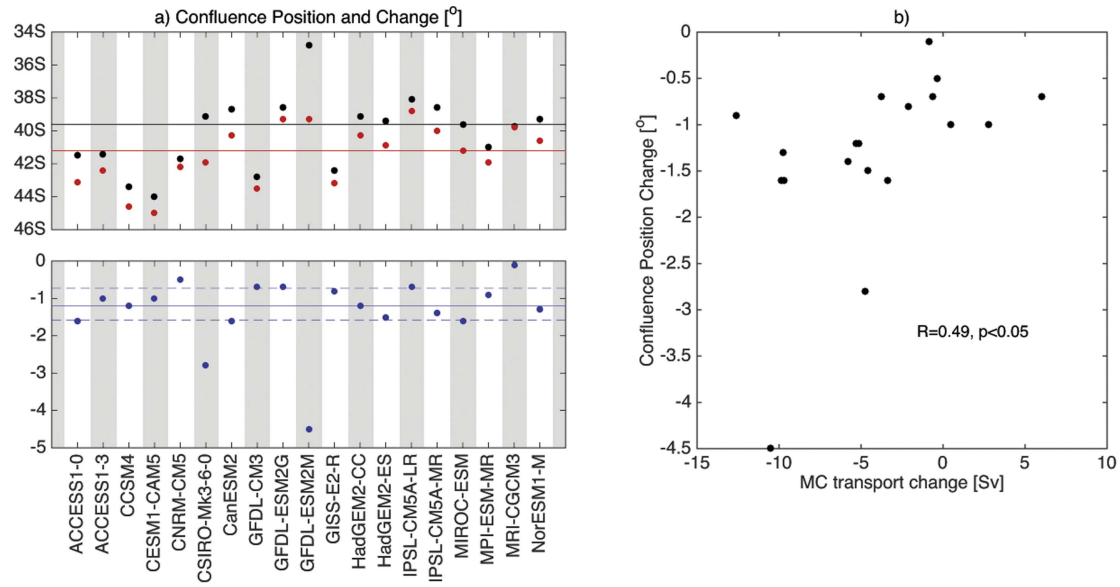

Figure 3. (a) Upper panel: confluence position for 20th century (black) and 21st century (red). Lower panel: confluence position change (RCP8.5 minus historical). Horizontal solid lines indicate multi-model medians and dashed lines indicate interquartile range. (b) Scatter plot between MC transport change (Sv) and confluence position change (°).

The projected change is greatest at around 39°S, poleward of the maximum mean state BC transport, with an intensification of 8.8 Sv (~5–11 Sv; figure 1(b)). In addition, 18 out of 19 models show a southward shift in the latitude of the maximum BC transport of ~1.2° (0.7°–1.5°; figure S4).

At 33°S, where the *historical* BC transport is strongest, the MMM projected intensification in the BC is largely compensated by a decrease in the NADW transport (figures 2(a) and (c)). However, even though the upper interior MMM change is not significant, inter model differences in BC transport are strongly related to differences in interior transport ($r = 0.81$, $p < 0.05$; table 1). At 38°S, close to where the BC intensification is strongest, the projected MMM BC intensification is associated with a complex set of changes to NADW, interior, other deep ocean transports and Indonesian throughflow (ITF) (figure 2(a)). However, the inter-model differences in the BC change is most strongly associated with changes in the upper interior transport across the Indo-Atlantic basin ($r = 0.95, p < 0.05$, table 1).

The North Brazil current (NBC) is the northward flowing branch of the South Equatorial current. In the historical simulations it shows an approximately linear increase from ~20°S to ~11°S reaching up to 20.5 Sv towards the north (17.5–26.7 Sv; figure 1(a)). This range lies within observational estimates at 11°S of 23–26 Sv (Hummels *et al* 2015; table S1). In the region north of 15°S the 21st century simulation shows a significant (>95%) decrease on NBC strength (figure 1(b)). The mean transport for 15°S–20°S is ~19 Sv (16–24.3 Sv; table S5). All but two models project a decrease in transport with a MMM of ~2.5 Sv (−4.7 to −1.4 Sv; table S5). At 10°S, the projected NBC decrease is largely compensated by changes in the NADW (~3 Sv; figure 2(a)) with a strong inter-model correlation ($r = 0.95, p < 0.05$; table 1).

At the southern extent of the Atlantic basin the powerful Malvinas current flows equatorwards fed by part of the ACC that migrates northwards as a result of topographic steering after transiting the Drake Passage (DP; figure S1). In the *historical* simulations the MC has a transport of 37.4 Sv (30–50.4 Sv) averaged between 50°S and 42°S. All but two models project a decrease in transport with a reduction of 3.7 Sv (6.7–1 Sv). This corresponds to a weakening of 8% (−12% to −3%). At 45°S the MC is projected to decrease by ~5 Sv, largely associated with a weakening of the upper ocean interior transport integrated across all basins ($r = 0.95, p < 0.05$; figure 2(a); table 1).

3.4. Brazil–Malvinas confluence (BMC)

Next we quantify the projected changes to the BMC and examine drivers that may give rise to changes in its position. We define the BMC position as the latitude where the meridional transport vanishes along the western boundary of the Atlantic basin. In order to better determine this latitude, the integrated western boundary meridional transport data was linearly interpolated to 0.1°. The simulated BMC is located at 39.6°S (38.8°–41.6°S; figure 3(a); equivalent to the latitude of zero transport in figure 1(a)—red solid line). By comparison the observed location is 38°S (from 1993 to 2008—Goni *et al* 2011, from 1992 to 2007—Lumpkin and Garzoli 2011). As such the BMC is systematically simulated too far to the south. In the warming scenario, all models project a southward shift in the mean BMC position of 1.2° (0.7°–1.6°; figure 3(a)).

To help understand the cause of the BMC latitudinal change we examine the various drivers that have been proposed in the literature: basin wide WSC (Lumpkin and Garzoli 2011), BC transport (Olson *et al* 1988), MC transport (Matano 1993, Combes and Matano 2014), and DP transport (Gan *et al* 1998). To examine the influence of the WSC, we look at the projected change in the latitude of the WSC zero line. Sverdrup theory suggests an interior divergence and an associated zonal flow fed from the WBCs at this latitude. To analyze the influence due to BC and MC transport, the meridional transport at latitudes 5° north and south, respectively, of each model's 20th century BMC position was related to the BMC position. For latitudes closer than this there may be aliasing of the two current as they can both exist at the same latitude (see schematic figure S1). The DP transport is calculated at 68°W.

Changes in the WSC zero line (which shifts southwards in all models), BC transport (which increases in all models) and MC transport (which decreases in 16 out of 19 models) are all consistent with the robust southward shift in the confluence position. However, based on a multiple linear regression (MLR) analysis using these potential drivers as predictors of mean BMC latitude (table S3) we find that the MC transport plays a primary role in explaining intermodel differences in the mean BMC position ($r = 0.79, p < 0.05$), followed by BC transport ($r = 0.5, p < 0.05$). This is in agreement with Matano (1993) who suggested that the BMC position is mainly related to the MC strength.

MLR is also used to examine inter-model differences in projected BMC latitude changes (table S4). Only the MC transport change has a significant relationship with the BMC position change ($r = 0.49$, $p < 0.05$; figure 3(b)). As such, intermodel differences in the projected shift in BMC can be partly associated with differences in projected MC transport changes. Adding the other variables as predictors of BMC change provides little additional benefit for predicting inter-model differences in the confluence position change (table S4). We would note that south of the BMC at 45°S there is no relationship between MC transport and the strength of the DP transport (although there is a weak relationship further south $r = 0.44, p = 0.05$ at 50°S). As noted, there is a strong relationship between projected MC change and the change in interior transport across all basins ($r = 0.95$; table 1; figure 2(a)), however the interior transport changes are unrelated to WSC changes via Sverdrup dynamics ($r < 0.1$).

4. Discussion and conclusions

Sverdrup theory relates WSC changes to changes in the basin interior meridional transport, in the absence of deep density driven circulation changes. Here we find that a projected decrease in the WSC between 15° S and 30°S indeed explains the ~20% reduction in northward upper ocean interior transport. However, there is no significant reduction in the WBC transport at this region, and the reduced interior transport is largely compensated by a reduction in the deep (>1000 m) southward transport. This is consistent with a weakening of NADW transport resulting from high latitude North Atlantic warming and freshening (Dong *et al* 2014), and with the projected northward anomalies in the abyssal circulation (figure 2(c)).

The southward shift in the WSC zero line and the weakening in the upper-ocean basin interior transport are likely to have important consequences to the world's ocean dynamics. The change in the WSC pattern drives a polewards shift of the frontal zone between the subtropical gyre circulation and the ACC, that leads an increased Agulhas leakage (Biastoch *et al* 2009). However, this change in the Agulhas leakage may not reflect an increased inter-hemispheric heat transport, as there is a projected decrease in both basin interior and North Brazil current volume transports: the primary pathways of this heat exchange.

There is a consistent and substantial intensification of the BC of almost 40% between 30° and 40°S. North of the southern tip of Africa the relatively weak BC increase is largely compensated by the NADW reduction with inter-model differences mainly associated with large differences in upper ocean interior transport related to changes in WSC. South of Africa, despite a decrease in the water entering the combined Indo-Atlantic region via ITF (figure 2(a); Sen Gupta *et al* 2016) there is a very large increase in the BC. This increased BC transport is primarily compensated by increases in the upper ocean interior Indo-Atlantic transport. However, changes in the Indo-Atlantic WSC and associated Sverdrup transport cannot explain these interior changes (intermodel correlation is not significant, table 1). This is unsurprising as this latitude intersects the location of the Agulhas current retroflection.

The location of the BMC is projected to shift southward by ~1.2°. The relationship between the ACC and MC transport, which can modulate the BMC position, and surface winds is not straightforward (Fetter and Matano 2008, Lumpkin and Garzoli 2011), especially due to the existence of a complex topography in the Drake Passage region. Despite southward shifts in the WSC pattern, we found that intermodel differences in the projected BMC southward shift location only showed a significant relationship with MC strength. This is consistent with findings of Combes and Matano (2014), who reported an observed southward shift of 0.62° decade^{-1} between 1993 and 2008 and related this to a weakening of the northern branch of the ACC and a consequent reduction of the MC transport. Moreover, results are consistent with Matano (1993) who used idealised experiments to show that the BMC is displaced

northwards of the WSC zero line by a strong MC, with BMC location modulated by the strength of the MC transport.

A key uncertainty in this analysis lies on the coarse resolution of the CMIP5 models. The models are unable to simulate the mesoscale processes that are important in this highly energetic region. Despite this, the gross changes described here should be constrained by basin wide wind changes. Indeed a similar analysis for the East Australian current (Oliver and Holbrook 2014) found very little difference between CMIP5 projections and projections from an eddy permitting model with regard to changes in the long-term transport of the WBCs. There is also considerable uncertainty with regards to the future evolution of the winds over the Southern ocean. This is related to compensating effects of greenhouse gases and the ozone forcing (e.g. Gillett and Fyfe 2013).

Our findings may have important consequences for regional climate and ecosystems. BC intensification can potentially increase heat and salt transport along the BC pathway, modifying the SST gradient that can affect regional weather in coastal areas (Pezzi *et al* 2005, De Camargo *et al* 2013). Additionally, Prado *et al* (2016) observed a decrease in the occurrence of temperate marine mammals between 30° and 34°S since 1970s, where we project a robust change in the BC. Thusly, the changes can potentially modify the distribution of marine species and affect economically local fishery production (e.g. Andrade 2003, Alemany *et al* 2014).

Acknowledgments

For their roles in producing, coordinating, and making available CMIP5 model output, we acknowledge the climate modeling groups (table S2), the World Climate Research Programme's Working Group on Coupled Modelling and the Global Organization for Earth System Science Portals. This work was supported by the National Council for Research Development (Brazil-CNPq) and the Australian Research Council (ARC) including the ARC Centre of Excellence in Climate System Science, and the NCI National Facility, Canberra.

References

Alemany D, Acha E M and Iribarne O O 2014 Marine fronts are important fi shing areas for demersal species at the Argentine Sea (Southwest Atlantic ocean) *J. Sea Res.* **87** 56–67

Andrade H A 2003 The relationship between the skipjack tuna (Katsuwonus pelamis) fishery and seasonal temperature variability in the South-Western Atlantic *Fisheries Ocanography* **12** 10–8

Barnes E A and Polvani L 2013 Response of the midlatitude jets, and of their variability, to increased greenhouse gases in the CMIP5 models *J. Clim.* **26** 7117–35

Biastoch A *et al* 2009 Increase in Agulhas leakage due to poleward shift of Southern Hemisphere westerlies *Nature* **462** 495–9

Bracegirdle T J *et al* 2013 Assessment of surface winds over the Atlantic, Indian, and Pacific ocean sectors of the Southern ocean in CMIP5 models: historical bias, forcing response, and state dependence *J. Geophys. Res.: Atmos.* **118** 547–62

Cai W *et al* 2005 The response of the Southern annular mode, the East Australian current, and the southern mid-latitude ocean circulation to global warming *Geophys. Res. Lett.* **32** 1–4

Combes V and Matano R 2014 Trends in the Brazil/Malvinas confluence region *Geophys. Res. Lett.* **41** 799–804

De Camargo R *et al* 2013 Modulation mechanisms of marine atmospheric boundary layer at the Brazil–Malvinas confluence region *J. Geophys. Res.: Atmos.* **118** 6266–80

Dong S *et al* 2014 Seasonal variations in the South Atlantic meridional overturning circulation from observations and numerical models *Geophys. Res. Lett.* **41** 4611–8

Fetter A F H and Matano R P 2008 On the origins of the variability of the Malvinas current in a global, eddy-permitting numerical simulation *J. Geophys. Res.* **113** C11018

Fligner M A and Policello G E 1981 Robust rank procedures for the behrens-fisher problem *Am. Stat. Assoc.* **76** 162–8

Gan J, Mysak L A and Straub D N 1998 Simulation of the South Atlantic ocean circulation and its seasonal variability *J. Geophys. Res.* **103** 241–51

Garzoli S L 1993 Geostrophic velocity and transport variability in the Brazil-Malvinas Confluence *Deep-Sea Research* I **40** 1379–403

Garzoli S L *et al* 2015 The fate of the deep western boundary current in the South Atlantic *Deep-Sea Res.* I **103** 125–36

Gillett N P and Fyfe J C 2013 Annular mode changes in the CMIP5 simulations *Geophys. Res. Lett.* **40** 1189–93

Goni G J, Bringas F and Dinezio P N 2011 Observed low frequency variability of the Brazil current front *J. Geophys. Res.: Oceans* **116** C10037

Gordon A L and Greengrove C L 1986 Geostrophic circulation of the Brazil–Falkland confluence *Deep Sea Res.* A **33** 573–85

Harvey B J, Shaffrey L C and Woollings T J 2014 Equator-to-pole temperature differences and the extra-tropical storm track responses of the CMIP5 climate models *Clim. Dyn.* **43** 1171

Hill K L, Rintoul S R, Coleman R and Ridgway K R 2008 Wind forced low frequency variability of the East Australia current *Geophys. Res. Lett.* **35** L08602

Hummels R *et al* 2015 Interannual to decadal changes in the western boundary circulation in the Atlantic at 11°S *Geophys. Res. Lett.* **42** 7615–22

Lentini C A D, Goni G J and Olson D B 2006 Investigation of Brazil current rings in the confluence region *J. Geophys. Res.* **111** C06013

Lu J, Vecchi G A and Reichler T 2007 Expansion of the Hadley cell under global warming *Geophys. Res. Lett.* **34** L06805

Lumpkin R and Garzoli S 2011 Interannual to decadal changes in the Western South Atlantic ' s surface circulation *J. Geophys. Res.* **116** 1–10

Matano R P 1993 On the separation of the Brazil current from the coast *J. Phys. Oceanogr.* **23** 79–90

Oliver O C J and Holbrook N J 2014 Extending our understanding of South Pacific gyre 'spin-up': modeling the East Australian current in a future climate *J. Geophys. Res.: Oceans* **119** 2788–805

Olson D B, Podesta G P, Evans R H and Brown O B 1988 Temporal variations in the separation of Brazil and Malvinas currents *Deep Sea Res.* A **35** 1971–90

Peterson R G and Stramma L 1991 Upper-level circulation in the South Atlantic ocean *Prog. Oceanogr.* **26** 1–73

Pezzi L P, Souza R B, Dourado M S, Garcia C A E, Mata M M and Silva-Dias M A F 2005 Ocean-atmosphere *in situ* observations at the Brazil–Malvinas confluence region *Geophys. Res. Lett.* **32** L22603

Polvani L M, Waugh D W, Correa G J and Son S W 2011 Stratospheric ozone depletion: the main driver of twentieth-century atmospheric circulation changes in the Southern Hemisphere *J. Clim.* **24** 795–812

Prado J H F, Matos P H, Silva K G and Secchi E R 2016 Long-term seasonal and interannual patterns of marine mammal

strandings in subtropical Western South Atlantic *PLos One* **11** e0146339

Saenko O A, Fyfe J C and England M H 2005 On the response of the oceanic wind-driven circulation to atmospheric CO_2 increase *Clim. Dyn.* **25** 415–26

Sen Gupta A, Santoso A, Taschetto A, Ummenhorfer C, Travena J and England M 2009 Projected changes to the Southern Hemisphere ocean and sea ice in the IPCC AR4 climate models *J. Clim.* **22** 3047–78

Sen Gupta A, Shayne M, Van Sebille A, Ganachaud A, Brown J and Santoso A 2016 Future changes to the Indonesian throughflow and Pacific circulation : the differing role of wind and deep circulation changes *Geophys. Res. Lett.* **43** 1669–78

Stramma L 1989 The Brazil Current transport south of 23ºS *Deep-Sea Res.* **36** 639–46

Taylor K E, Stouffer R J and Meehl G A 2012 An overview of CMIP5 and the experiment design *Bull. Am. Meteorol. Soc.* **93** 485–98

Wainer I, Gent P and Goni G 2000 Annual cylce of the Brazil–Malvinas confluence region in the National Center for Atmosphere Research Climate System Model *J. Geophys. Res.* **105 26** 167–77

Wainer I, Taschetto A, Otto-Bliesner B and Bardy E 2004 A numerical study of the impact of greenhouse gases on the South Atlantic Ocean climatology **66** 163–89

Wu L *et al* 2012 Enhanced warming over the global subtropical western boundary currents *Nat. Clim. Change* **2** 161–6